

6th CIRP Conference on Surface Integrity

Numerical modelling of the drag finishing process at a macroscopic scale to optimize surface roughness improvement on additively manufactured (SLM) Inconel 718 parts

Irati Malkorra^{a,b*}, Hanène Souli^a, Ferdinando Salvatore^a, Pedro Arrazola^c, Joel Rech^a, Aude Mathis^d, Jason Rolet^b

^aUniversity of Lyon, Ecole Centrale de Lyon - ENISE, LTDS CNRS UMR 5513, 58 Rue Jean Parot, 42000, Saint-Etienne, France

^bIRT-M2P, 4 Rue Augustin Fresnel, 57070, Metz, France

^cFaculty of Engineering, Loramendi 4, Mondragon University, 2500, Arrasate, Spain

^dNaval Group, CESMAN, Technocampus Ocean, 5 rue de l'Halbrane, 44340, Bouguenais, France

* Corresponding author. E-mail address: irati.malkorra@gmail.com

Abstract

Drag finishing is one of the mass finishing processes that enhances surface roughness on complex and rough parts produced by additive manufacturing. This paper proposes a model to simulate abrasive media flowing around the part at a macroscopic scale based on an original rheological model inspired by civil engineering techniques. The correlation between the evolution of the surface roughness and numerical results reveals the high sensitivity of the process to media's rheological behaviour and the surface orientation of the surface regarding media flow. This model provides a better understanding of the physical mechanisms (chip formation or plastic deformation) induced at the surface during polishing, and it helps choosing the optimal finishing conditions.

© 2022 The Authors. Published by Elsevier B.V.

This is an open access article under the CC BY-NC-ND license (<https://creativecommons.org/licenses/by-nc-nd/4.0>)

Peer review under the responsibility of the scientific committee of the 6th CIRP CSI 2022

Keywords: Polishing, Drag finishing, Surface roughness, Rheology, Numerical simulation

1. Introduction

Drag finishing is a mass finishing technique that improves the surface roughness of a component external surfaces. Parts are clamped on a spindle and submerged into a mixture of abrasive media and liquid compound. A drag motion is then applied to the part (rotations w_1 & w_2 in Fig. 1a) [1]. The relative movement between the abrasive media and surface during polishing improves surface roughness due to abrasive mechanisms. This process has received limited attention from the scientific community, compared to other finishing processes. The optimisation of this process is mainly based on empirical knowledge and necessitates several trial-and-error tests to reach the desired surface roughness all around a

complex part. However, drag finishing becomes more popular with the development of complex 3D printed parts having very rough surfaces in their as-built state. Such parts are very costly and are produced in small batches, so it becomes highly necessary to predict the best processing conditions before starting the effective post-treatment. Today, the modelling of drag finishing, i.e. the prediction of surface roughness evolution all around a part, remains an issue. At a macroscopic scale, the mass of the media can be considered as a continuous material flowing around the part (Fig. 1b). Although modelling of other mass finishing processes, such as vibratory finishing [2] have been addressed in the past, there is not any research work dealing with the modelling of drag finishing at this scale and taking into account the interaction with the part to polish.

At a mesoscopic scale, more scientific works have addressed the modelling of mass finishing processes (not only drag finishing). At this scale, media are considered as rigid bodies (Fig. 1c) and the interactions between them (friction and interlocking effect) and with the part are commonly simulated with Discrete Element Models (DEM) [3].

At a microscopic scale, the interaction between a single medium and the surface with a complex topography (roughness) has been largely researched for several abrasive processes (Fig. 1d) [4,5].

The three scales are strongly coupled together. However, the industrial need to predict the evolution of surface roughness around a real complex part requires a model at the macroscopic scale.

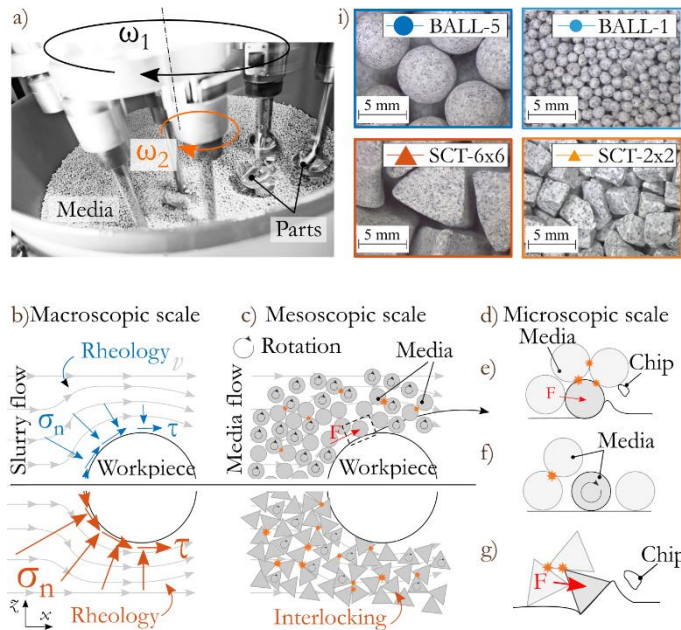


Fig. 1. a) Drag finishing machine, b to g) illustration of the multi-scales, i) investigated four types of media

Recently, Malkorra [6] proposed the first drag finishing model that considers media flow as an homogeneous slurry flowing around the part being polished. The approach was applied to the drag finishing of AISI1045 pre-machined samples with two different media. The correlation between the numerical contact conditions and the evolution of surface roughness enabled to highlight the effective abrasive mechanisms (chip formation or plastic deformation) leading to the improvement of surface roughness over the part. Hence, it enables the definition of the best media and the best drag finishing conditions.

The present paper aims to investigate and optimise the surface roughness improvement on a rough Inconel 718 cylindrical part produced by Selective Laser Melting (SLM) (Fig. 2a). The selection of abrasive media is the dominant parameter [5-7] and thus, four abrasive media of 2 shapes (sphere and pyramid) and 2 sizes with similar compositions (alumina grain size and ceramic binder) have been investigated (Fig. 1i).

After a presentation of the numerical drag finishing model, the rheological properties of the four abrasive media are characterised. The simulations of the four drag finishing conditions are correlated to the evolution of surface roughness over a cylindrical sample, which reveals the optimal drag

finishing conditions and the corresponding abrasive mechanisms (chip formation or plastic deformation).

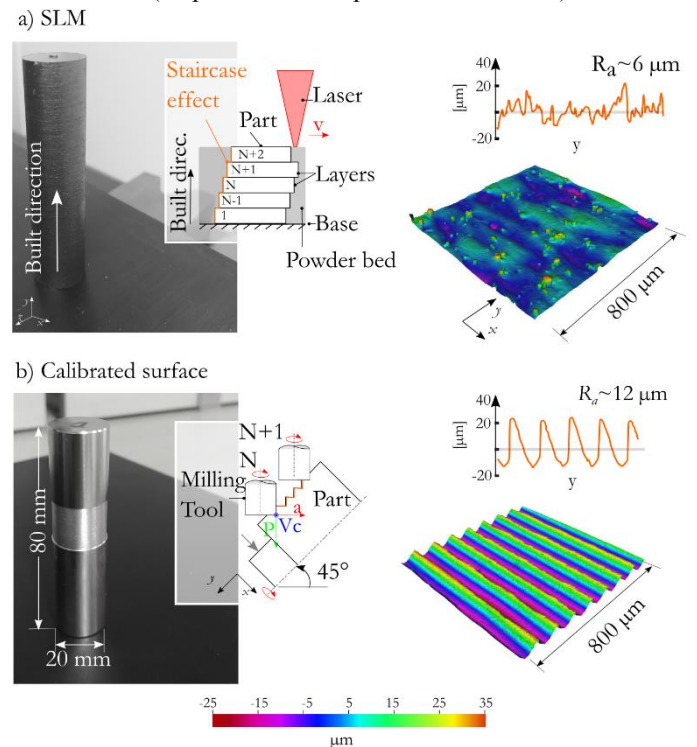


Fig. 2. a) Inconel718 SLM samples, b) machined samples

2. Description of the numerical model

The FE model of the drag finishing process is presented in Fig. 3. The part to be polished has a cylindrical shape and is immersed into the media, which is considered as a homogeneous material (slurry) presenting a specific rheological property. The part has a simplified kinematic with a single circular movement (ω_1) (Fig. 3a) (without rotation around its own axis). Consequently, the interaction between the media and the surface depends on the orientation angle of the surface (α) (Fig. 3b).

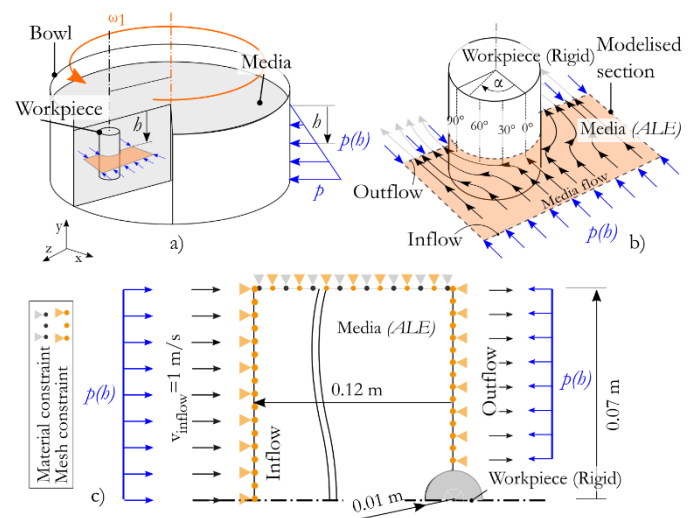


Fig. 3. a) Simplified drag finishing set-up with one rotation, b) media flow around a cylindrical part and c) a detailed description of the 2D ALE model.

The Finite Element Model (FEM) is based on an Arbitrary

Lagrangian Eulerian (ALE) formulation that provides the contact conditions between the slurry and the surface, i.e. the normal stress (σ_n), the shear stress (τ) and the sliding velocity (v).

The model considers a 2D plain strain section located at an immersion depth (h) (Fig. 3a). This induces a hydrostatic pressure $p(h)$ on the media (Fig. 3b and 3c). The part is considered to be rigid and the media flow enters through the inflow section.

The inflow velocity is kept constant at 1 m/s, corresponding to the maximum velocity of the experimental set-up. The model is based on plane strain elements (CPE4R) in ABAQUS Explicit. A kinematic contact algorithm with a Coulomb friction coefficient of $\mu=0.3$ is employed to define the contact interaction.

3. Rheological properties of abrasive media

Abrasive media have similarities with soils in civil engineering, as they are composed of a large number of solid particles (stones=media) and a cohesive phase (mud=liquid compound). When considering this abrasive slurry as a homogeneous material at a macroscopic scale, the Drucker Prager rheological equations are commonly used (Eq.1 to 3) [7]. This model is pressure dependent, in which p and q are pressure and equivalent stress invariants. The bulk density (ρ_{bulk}), Young's modulus (E), Poisson's ratio (ν), internal friction angle (φ), dilatancy angle (ψ) and the ratio between the yield stress in triaxial tension to triaxial compression (K) are needed to define this plasticity model. The yield limit is defined by Eq.1 and the asymmetry between tension and compression is calculated by Eq.2. The hardening of the material is defined in uniaxial compression and the flow potential is expressed by Eq. 3.

$$f = t - p \tan \varphi - c = 0 \quad \text{Eq. 1}$$

$$t = \frac{1}{2}q \left[1 + \frac{1}{K} - \left(1 - \frac{1}{K} \right) \left(\frac{r}{q} \right)^3 \right] \quad \text{Eq. 2}$$

$$G = t - p \tan \psi \quad \text{Eq. 3}$$

Triaxial tests (Fig. 4) were carried out to define the parameters of the rheological model, following the procedure explained in [8]. These tests consist of surrounding an amount of media with a deformable membrane and confining it under a pressure (σ_3). Then an additional pressure (σ_1) is applied to shear the sample. During the tests, the stresses and vertical and radial deformations (ε_y , ε_v) of the sample are tracked, and material rheological properties are calculated (such as E , ν , φ and ψ) based on the graphical analysis described in [6].

Table 1 reports the rheological properties of the four types of media that were characterised (Fig. 1i). It appears that pyramidal media (SCT 6×6 and SCT 2×2) present a higher Young's modulus (E), internal friction angle (φ) and dilatancy angle (ψ) than the spherical media (BALL-5 and BALL-1). This means that the drag force applied to the part will be higher and, consequently, higher mechanical stresses will be applied on the surface during polishing. This is due to the interlocking effect between media as they have an angular shape (Fig. 1c).

The effect of media size seems clear in the case of pyramidal media: the larger the media, the higher the mechanical resistance. On the contrary, this trend is not so clear as far as spherical media are concerned. Indeed, the Young's modulus (E) of BALL-5 is larger but the internal friction angle (ψ) is lower than BALL-1. Both properties have an opposite effect on the drag force. The implementation of both rheological equations will enable discrimination of the influence of the size of spherical media.

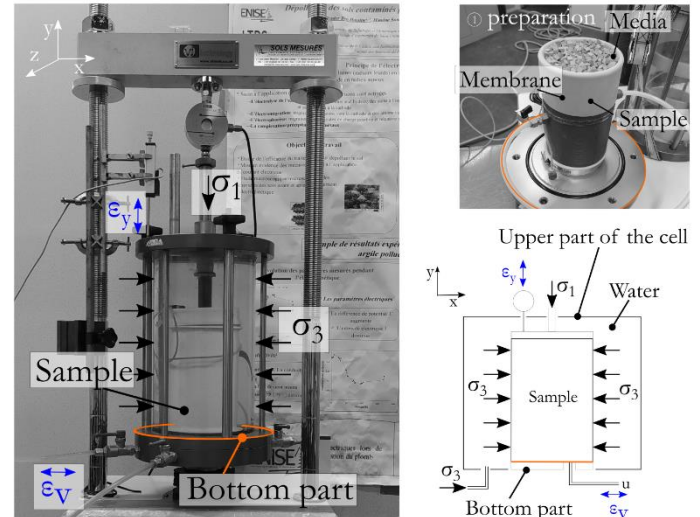


Fig. 4. Rheological tests on abrasive media.

Table 1
Rheological properties of medias (from triaxial tests)

Media	ρ_{bulk} [kg/m ³]	E [Pa]	ν [-]	φ [°]	ψ [°]
BALL-5	1713 ± 63	179000 ± 65	0.3 ± 0.1	31 ± 2	8 ± 3
BALL-1	1587 ± 49	80000 ± 80	0.27 ± 0.17	33 ± 2	7 ± 6
SCT 6×6	1489 ± 84	415000 ± 49	0.46 ± 0.07	45 ± 1	13 ± 1
SCT 2×2	1667 ± 60	354000 ± 29	0.43 ± 0.1	40 ± 1	11 ± 3

4. Experimental drag finishing tests

The objective of this work is to optimise the drag finishing conditions on Inconel 718 parts produced by SLM. So, cylindrical samples were manufactured ($\text{Ø}20 \times \text{L}80$ mm) (Fig. 2a). The surfaces of these parts are not homogeneous and vary from one sample to another. Surfaces were measured by means of a focus variation microscope (magnification x20, vertical and lateral resolutions: 2.5 and 0.1 μm). The initial arithmetic mean height of the roughness ($S_a \sim 6 \mu\text{m}$) was quantified by the MountainMaps software after applying a form SL-filter, in accordance with ISO25718. The evolution of S_a was quantified during drag finishing and plotted in Fig. 5(a) for four orientation angles (α): front ($\sim 0^\circ$), intermediate ($\sim 30^\circ$ and $\sim 60^\circ$) and lateral ($\sim 90^\circ$).

One of the objectives of this work is also to determine the abrasive mechanisms (material removal or plastic deformation) involved in drag finishing, depending on the orientation angle (α) around the sample and on the geometry of abrasive media. As shown by [6], it is possible to discriminate these mechanisms by superimposing the evolution of surface roughness profiles. The complexity and the variability of roughness profiles over a sample and among the samples make

this analysis impossible in SLM samples (Fig. 6b). So, in addition to SLM ones, samples with a defined surface roughness profile have also been manufactured by milling (Fig.2b). The milling operation, described in [5,8], enables a homogeneous surface of $Sa \sim 15 \mu\text{m}$ in all samples. The evolution of the roughness (Sa) and profile positions were tracked during drag finishing and plotted in Fig. 5(b) for various orientation angles (α).

5. Results and discussion

Fig. 5(a) and 5(b) plot the evolution of the roughness parameter (Sa) for SLM samples and for machined samples, respectively. Only three orientation angles have been plotted, as the results for intermediate areas ($\alpha \sim 30^\circ$ and $\alpha \sim 60^\circ$) are very similar. As expected, the surface roughness is systematically improved but not with the same magnitude, depending on the orientation angle and on the type of media. The trends for both families of samples (SLM and machined) are similar and thus, this section will focus on the analysis of the machined samples, as the fundamental abrasive mechanisms appear more clearly.

It is worth noting that the slopes of the curves are much more intense for machined samples than for SLM samples. One of the reasons for this is linked to the higher level of initial roughness ($Sa \sim 15$ versus $6 \mu\text{m}$) and the sharpness of peaks as far as machined surfaces are concerned.

Fig. 6 shows the initial and final surface profiles for machined samples after 120 min of drag finishing. An overview of this figure shows that the original calibrated roughness profile may be either fully removed or only slightly affected on peaks, depending on the orientation angle and on the type of media.

Finally, the numerical simulations of drag finishing at the macroscopic scale for the four types of media provide the distribution of the mechanical loadings (Fig. 7), i.e. the normal stress (σ_n), the shear stress (τ) and the sliding velocity (v) around the samples, from the frontal area ($\alpha \sim 0^\circ$) to the lateral

area ($\alpha \sim 90^\circ$). An overview of this figure reveals that the distribution of the loading strongly depends on the orientation of the surface and differs significantly between the four media. It shows that the normal stress (σ_n) is at a maximum in the frontal zone ($\alpha \sim 0^\circ$), whereas the shear stress (τ) is at a maximum in an intermediate area ($\alpha \sim 20^\circ$). As far as the sliding velocity (v) is concerned, the simulation estimates that a stagnation area exists in the frontal zone. This numerical result has no meaning when considering the physical phenomena at a

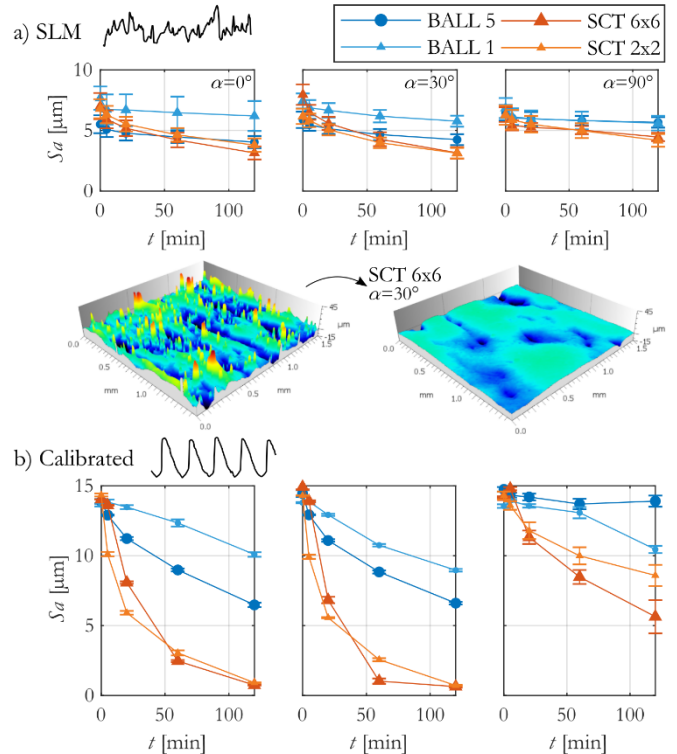


Fig. 5. Surface roughness (Sa) evolution for various orientation angles ($\alpha = 0, 30$ and 90°) for SLM parts (a) and machined parts (b).

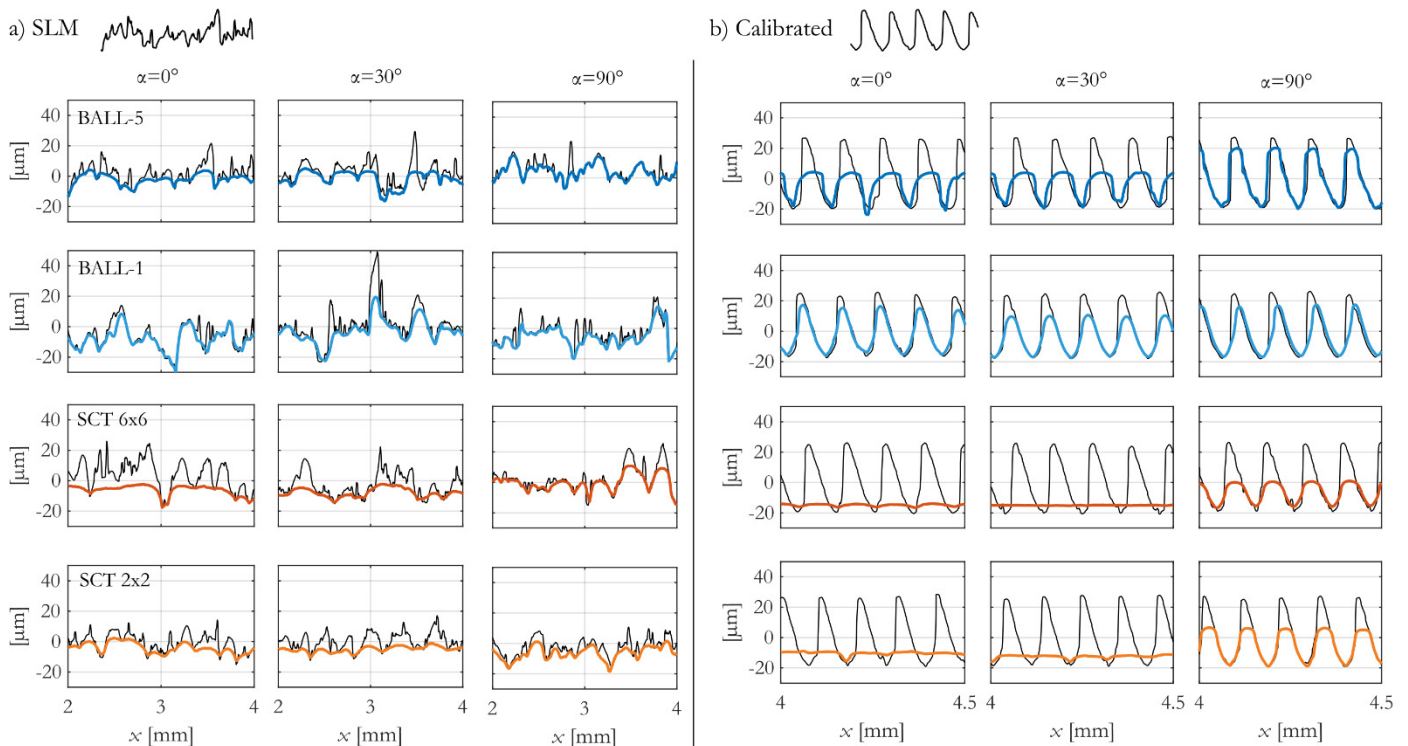


Fig. 6. Surface roughness profiles before and after 120 min. of drag finishing for three orientation angles and four geometries of medias.

mesoscopic scale (Fig. 1c). At this scale, the interaction between individual media (friction and interlocking phenomena) prevents any stagnation. This error comes from the assumption of considering a continuum and a homogeneous material. However, the sliding velocity is small in this frontal area. On the contrary, this parameter becomes a maximum around $\alpha \sim 60^\circ$. It then decreases suddenly, when reaching $\alpha \sim 90^\circ$, as the contact between the slurry and the part is lost because of the high viscosity of the material. Only the small ball media are able to maintain the contact till $\alpha \sim 90^\circ$ due to its low rheological properties.

The correlation between Fig. 5 to 7 reveals three main trends: **Firstly**, surfaces in the frontal ($\alpha \sim 0^\circ$) and intermediate ($\alpha \sim 30^\circ$ and $\alpha \sim 60^\circ$) areas are more efficiently polished than in the lateral area ($\alpha \sim 90^\circ$) (Fig. 5b). This is confirmed by Fig. 6, where the magnitudes of roughness profiles are much more reduced for $\alpha \sim 0^\circ$ and 30° . This statement can be correlated to the mechanical loadings around the part. The frontal ($\alpha \sim 0^\circ$) and intermediate ($\alpha \sim 30^\circ$) areas withstand much more intense normal (σ_n) and shear (τ) stresses, compared to the lateral zone (Fig. 7). A slightly better surface finish can be obtained for intermediate orientation angles ($\alpha \sim 30^\circ$), which can be correlated to the maximum shear stress in this area. On the contrary, there does not seem to be any correlation between the sliding velocity and the surface roughness improvement in this application.

The improvement of surface roughness can be induced by two mechanisms: material removal or plastic deformation. As shown by [6], when severe plastic deformation becomes the dominant mechanism, peaks are shifted downwards and valleys upwards, so as to keep the volume of material. As far as the spherical media are concerned, Fig. 6 shows that they have only removed the peaks of the roughness profiles, without affecting the valleys. This reveals that spherical media are not able to induce a significant plastic deformation in Inconel718 surfaces. As far as pyramidal media are concerned, a similar conclusion can be proposed based on the analysis of roughness profiles for the lateral area ($\alpha \sim 90^\circ$). Therefore, material removal from roughness peaks seems to be the dominant mechanism and plastic deformation is not significant, irrespective of the orientation angle and the type of media. The material removal mechanism seems to be correlated to the level of mechanical stress applied on the surface.

Secondly, regardless of surface orientation (α), pyramidal media are more efficient at decreasing surface roughness than spherical ones. This is especially clear in Fig. 5(b). Fig. 6 highlights that pyramidal media have almost removed the initial roughness profiles for the frontal ($\alpha \sim 0^\circ$) and intermediate ($\alpha \sim 30^\circ$) areas, whereas spherical media have only removed the peaks. Apart from the analysis of roughness profiles, the observation of mechanical loadings in Fig. 7 shows that pyramidal media lead to high normal (σ_n) and shear stresses (τ). For instance, the biggest pyramidal media (SCT6 \times 6) induced normal stresses (σ_n) up to 45 kPa, whereas the biggest spherical media (BALL-5) only induced 20 kPa. These observations are directly linked to the higher rheological properties of pyramidal media, as described in section 3. Indeed, contrary to spherical media, the interlocking phenomena between pyramidal media prevent any rotation at

the mesoscopic scale (Fig. 1c). Consequently, at a microscopic scale, when a pyramidal media approaches the surface to polish, the media can hardly change its orientation, which facilitates the generation of chips (Fig. 1g). As far as spherical media are concerned, they can either rotate (Fig. 1f) on the surface or scratch the surface (Fig. 1e). The rotation of a single media is only limited by the friction coefficient in the contact areas with its neighbours. The friction force is directly linked to the normal contact force. So, when a high stress is applied, the scratch mechanism dominates (Fig. 1e). This explains why the surface roughness is more efficiently improved for low orientation angles where stresses are more important.

Thirdly, the biggest trend is the media size, the larger it is, the smoother the surface (Fig. 5b). This trend is especially visible for pyramidal media (SCT6 \times 6 and SCT2 \times 2) in the lateral area ($\alpha \sim 90^\circ$) (Fig. 6), where the peaks of initial profiles are much more decreased. This observation can be correlated to the mechanical loadings applied on the surface (Fig. 7). It is obvious that normal (σ_n) and shear stresses (τ) are much higher for the biggest media, and this is linked to its higher rheological behaviour.

A similar trend is observable for spherical media. The largest media (BALL-5) are able to remove more material on the peaks, compared to small ones (BALL-1) in the frontal and intermediate areas (Fig. 5b). However, the mechanical loadings are very similar. This shows that the macroscopic rheological properties of spherical media and the corresponding drag simulation are not able to provide a physical explanation for this statement. An additional model at the mesoscopic or microscopic scale should be developed to provide complementary explanations.

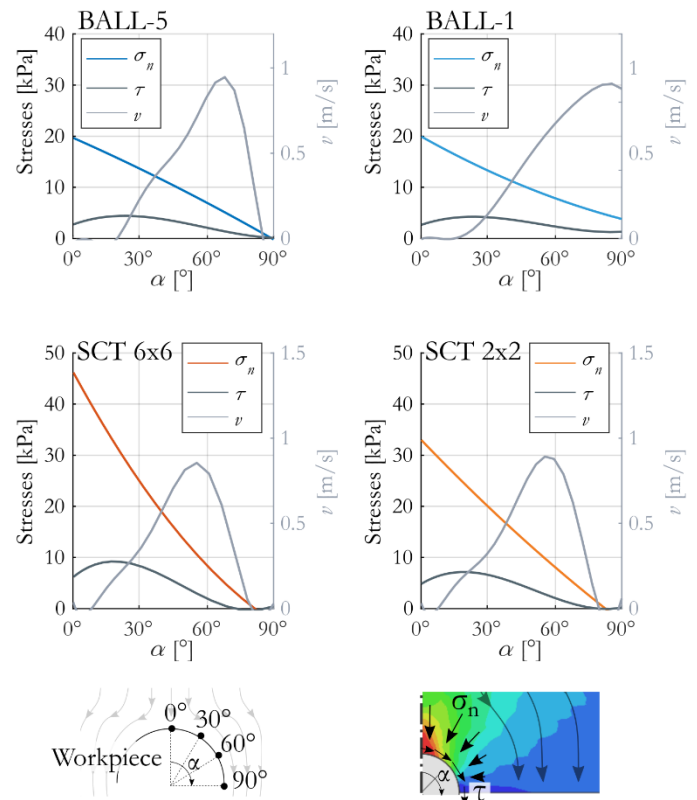


Fig. 7. Mechanical parameters around the cylindrical part for the 4 medias

6. Conclusion

This work aimed to optimise the drag finishing conditions to polish rough Inconel 718 parts produced by SLM. A 2D Finite Element Model using the ALE approach is employed to model the drag finishing process at the macroscopic scale. The abrasive media is considered as homogeneous slurry flowing around a part and its rheological properties are identified using in techniques employed for soil mechanics in civil engineering. Simulations provide the mechanical loadings induced at the interface between abrasive media and the surface. The correlation between the mechanical loadings and the evolution of surface roughness around a cylindrical part enables highlighting of the optimal drag finishing conditions and the corresponding fundamental abrasive mechanisms.

It has been shown that the shape and size of media are the key factors that influence their rheological properties at a macroscopic scale. Moreover, they will determine the magnitude of the mechanical loading applied on the surface to polish. The loading varies all around the part, with regard to the orientation of local surfaces. By analysing surface roughness profiles, it has been shown that material removal is the dominant mechanism. By comparing experimental and numerical results, it has been highlighted that surface roughness improvement is only correlated to mechanical stresses and not to sliding velocity. Therefore, this work has shown that the optimal drag finishing conditions to improve the surface on rough SLM surfaces can be obtained when using large pyramidal media and intermediate orientation angles.

Acknowledgements

Authors thank the IRT-M2P for the financial support.

References

- [1] Gillespie, L. K., 2007, *Mass Finishing Handbook*. New York: Industrial Press Inc.
- [2] Mullany, B., Shahinian, H., Navare, J., Azimi, F., Fleischhauer, E., et al., 2017, The application of computational fluid dynamics to vibratory finishing processes, *CIRP Annals*, 66/1:309–312, DOI:10.1016/J.CIRP.2017.04.087.
- [3] Zanger, F., Kacaras, A., Neuenfeldt, P., Schulze, V., 2019, Optimization of the stream finishing process for mechanical surface treatment by numerical and experimental process analysis, *CIRP Annals*, 68/1:373–376, DOI:10.1016/J.CIRP.2019.04.086.
- [4] Makiuchi, Y., Hashimoto, F., Beaucamp, A., 2019, Model of material removal in vibratory finishing, based on Preston's law and discrete element method, *CIRP Annals*, 68/1:365–368, DOI:10.1016/J.CIRP.2019.04.082.
- [5] Hashimoto, F., Yamaguchi, H., Krajnik, P., Wegener, K., Chaudhari, R., et al., 2016, Abrasive fine-finishing technology, *CIRP Annals - Manufacturing Technology*, 65/2:597–620, DOI:10.1016/j.cirp.2016.06.003.
- [6] Malkorra, I., Souli, H., Claudin, C., Salvatore, F., Arrazola, P., et al., 2021, Identification of interaction mechanisms during drag finishing by means of an original macroscopic numerical model, *International Journal of Machine Tools and Manufacture*, 168:103779, DOI:10.1016/j.ijmactools.2021.103779.
- [7] Hashemnia, K., Spelt, J. K. J. K., 2015, Finite element continuum modeling of vibrationally-fluidized granular flows, *Chemical Engineering Science*, 129:91–105, DOI:10.1016/j.ces.2015.02.025.